A&A 366, 294–305 (2001)
DOI: 10.1051/0004-6361:20000204

Astronomy & Astrophysics

The analysis of hard X–ray radiation of flares with occulted footpoints

M. Tomczak

Astronomical Institute, Wrocław University, Kopernika 11, 51-622 Wrocław, Poland
e-mail: tomczak@astro.uni.wroc.pl

Received 30 May 2000 / Accepted 26 October 2000

Abstract. 14 behind-the-limb flares with occulted footpoints, well-observed by *Yohkoh*, have been carefully selected. Such a flare location on the Sun offers a unique possibility to investigate loop-top hard X–ray emission sources separately, without the presence of strong footpoint sources which can disturb the observational characteristics of the loop-top sources during any process of image reconstruction. Hard X–ray radiation in all investigated flares has similar features: (1) smooth light curves with several impulsive spikes, (2) low-energy spectra (mainly below 33 keV) which can expressed in terms of temperatures within the interval of about 20–100 MK. The HXR images show two types of loop-top emission sources: type A, co-spatial with the bright loop-top kernels seen in soft X–rays, and type B, having no distinct counterpart in soft X–rays. Arguments are presented that this classification is more physical than the classification considering impulsive and gradual sources proposed by Masuda (1994), who actually separated two phases of evolution of the same loop-top source. The model of the turbulent flare kernel (Jakimiec 1998; Jakimiec et al. 1998) has been adapted to explain the obtained characteristics of loop-top HXR emission sources of type A.

Key words. Sun: corona – flares – X–rays, gamma-rays

1. Introduction

The discovery of impulsive loop-top hard X–ray (HXR) emission sources (Masuda 1994; Masuda et al. 1994, 1995) is one of the most important results of the *Yohkoh* mission. Although the sources show different observational properties (Masuda 1994), the loop-top source detected during the impulsive phase of the M2.0 flare of 13 January 1992, often called "the Masuda flare", has been considered to be a typical example. This source was located well above the apex of the soft X–ray (SXR) loop, where the bright loop-top kernel was developed, inside a high-temperature region seen in a temperature map derived from the Soft X–ray Telescope (SXT) images. The reported source had an impulsive time profile similar to that of the footpoint HXR sources. Its HXR energy spectrum, derived from the Hard X–ray Telescope (HXT) images which were synthesized within approximately 40-s time period starting from 17:26:52 UT, showed high-energy characteristics: 203 MK temperature (if a thermal model is assumed) or single power-law distribution with the index of 2.6 (if a non-thermal model is assumed). The simultaneously observed two HXR emission sources at footpoints were about five times stronger but had similar spectra.

Metcalf et al. (1996) pointed out that the quality of HXT images can be spoiled by spurious sources, especially in the case of weak sources having a low signal-to-noise ratio. Therefore, they have applied for the HXT image reconstruction the pixon algorithm (Piña & Puetter 1993) which gives fewer spurious sources than the classical Maximum Entropy Method. Using the pixon algorithm Alexander & Metcalf (1997) have repeated the HXT image reconstruction for the Masuda flare. These authors have confirmed the existence of the high-energy loop-top source, but they note that analysis of this source requires long integration times ($\sim$ a few tens of second) due to poor statistics. As a consequence, it is impossible to investigate the impulsive behavior of this source.

For several years investigations of many researchers aimed to propose a consistent physical model which would be able to explain all observational aspects of the Masuda flare (e.g. Shibata et al. 1995; Tsuneta 1996; Aschwanden et al. 1996a; Tsuneta et al. 1997; Hori et al. 1997; Yokoyama & Shibata 1998). Nevertheless, there is no commonly accepted model of this flare. The main problem is matching the features of the impulsive loop-top HXR emission source with other observations.

This may be due to instrumental reasons, i.e., the HXT image reconstruction methods may distort the actual parameters of the impulsive loop-top HXR emission source. Alexander & Metcalf (1997) identified the effect of weak source suppression during the HXT image reconstruction

Table 1. List of investigated behind-the-limb flares with occulted footpoints

No.	Date	GOES data			Location	NOAA AR	Number of degrees behind the solar limb	Height [km] of the SXR loop-top kernel	References
		Time of max	Class	Duration [min]					
1	21-Oct.-91	12:56	C7.8	20	S13 Elimb	6891	3°	$4\ 10^3$	a, b
2	10-Dec.-91	04:04	C9.3	20	S14 Elimb	6968	3°	$4\ 10^3$	
3	13-Jan.-92	19:13	M1.3	100	S10 Elimb	7012	5°	$1.0\ 10^4$	
4	6-Feb.-92	21:02	M4.1	140	N05 Wlimb	7030	4°	$1.0\ 10^4$	
5	19-Feb.-92	14:58	C9.2	30	N06 Elimb	7070	5°	$7\ 10^3$	
6	18-Jul.-92	13:44	M2.0	25	S11 Wlimb	7222	$> 0°$	$> 4\ 10^3$	
7	24-Nov.-92	10:05	C6.9	60	S07 Wlimb	7342	5°	$7\ 10^3$	c
8	24-Nov.-92	14:29	C5.9	80	S07 Wlimb	7342	7°	$1.0\ 10^4$	c
9	24-Nov.-92	16:04	C5.4	75	S07 Wlimb	7342	8°	$1.4\ 10^4$	c
10	24-Nov.-92	20:38	C6.4	140	S07 Wlimb	7342	10°	$1.9\ 10^4$	c
11	1-Feb.-93	02:04	M2.2	110	S10 Elimb	7416	6°	$7\ 10^3$	a
12	11-Nov.-93	11:26	C9.7	40	N10 Elimb	7618	5°	$8\ 10^3$	d
13	29-Jan.-94	11:29	M2.4	65	N07 Wlimb	7654	7°	$1.8\ 10^4$	a
14	29-Jan.-94	13:08	C6.5	55	N07 Wlimb	7654	8°	$1.6\ 10^4$	

[a] Mariska et al. (1996).
[b] Mariska & Doschek (1997).
[c] Khan et al. (1995).
[d] Ohyama & Shibata (1997).

and found that even the best method of reconstruction cannot eliminate it completely. They warned that due to this effect the ability to study the weak sources of HXR emission in the presence of strong sources is problematic. This applies to the impulsive phase of the majority of flares, e.g. the Masuda flare, where the footpoints sources are distinctly stronger than the loop-top source.

As long as the available methods of the HXT image reconstruction cannot eliminate completely the effect of weak source suppression, the only safe way to study the impulsive loop-top hard X–ray emission sources in detail is to exclude somehow the stronger sources. In the case of the behind-the-limb flares the solar limb works as a screen which occults the lower part of the flaring structure and leaves emission of the higher part only.

Several papers analyzing individual behind-the-limb flares have been published (Khan et al. 1995; Mariska et al. 1996; Sterling et al. 1996; Mariska & Doschek 1997; Ohyama & Shibata 1997; Mariska & McTiernan 1999). The authors based their analyses mainly on the *Yohkoh*/Bragg Crystal Spectrometer (BCS) data. The main goal of this paper is to use such a specific geometrical configuration for a closer look at the loop-top HXR emission sources using the HXT data.

2. The hard X–ray light curves

14 behind-the-limb flares with occulted footpoints, well-observed by *Yohkoh*, have been carefully selected (Table 1). None of these events coincides in time with another flare. This ensures that the observations of the whole-Sun instruments (*Yohkoh*/BCS, CGRO/BATSE, GOES) can be used for additional investigation of the loop-top area. The LDE events lasting longer than 2.5 hours have been omitted in this paper.

To estimate the actual height of the flaring structure, a projection along the line-of-sight has been calculated. For this purpose, a plot time-versus-longitude for all flares in the active region during its solar disc passage before or after the investigated flare has been made (Masuda 1994). A linear fit to this plot allows us to estimate the longitude of the behind-the-limb event (see Table 1).

For events from Table 1 it is reasonable to assume that the total hard X–ray radiation detected by the HXT comes from the loop-top area. This offered an unique chance to derive some parameters of loop-top HXR emission sources without the necessity of image reconstruction. Because of this, the obtained results have a better time resolution, up to the data sampling (0.5 s) and are not charged with the errors of the image reconstruction method.

In spite of the physical variety of the investigated flares, their HXR light curves show evident similarity. First, most of the emission occurs in the low energy channels: L (14–23 keV) and $M1$ (23–33 keV), only exceptionally reaching higher energy bands: $M2$ (33–53 keV), and H (53–93 keV) – see Table 2. Second, the light curves show two kinds of variability: a slow, long-term variability and a rapid, short-term variability (see Figs. 1 and 2).

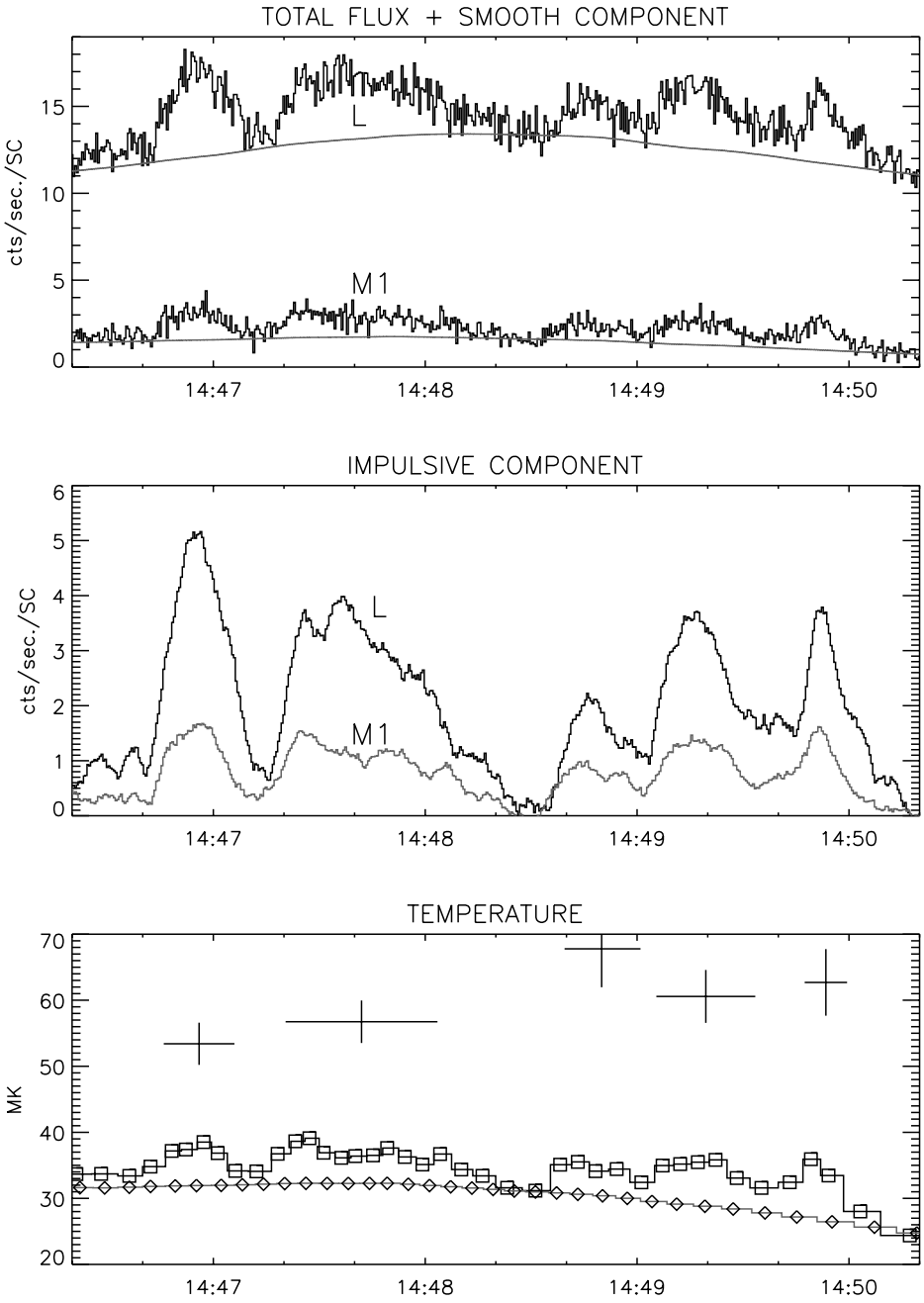

Fig. 1. The HXT light curves of the 19 February 1992 flare (event No. 5) in the channels L and $M1$ are presented. The background was subtracted. The 4-minutes interval around the maximum was selected when impulses were the strongest. The top panel contains plots of the total flux, $f_{\rm T}$, and of the smooth component, $f_{\rm S}$. In the middle panel plots of the impulsive component, $f_{\rm I}$, are shown. To lower a statistical noise in the case of this component the light curves were smoothed by central-moving-averages of 5 s duration. The temperatures estimated from the $M1/L$ hardness ratio are marked in the bottom panel by boxes, diamonds, and error bars for $f_{\rm T}$, $f_{\rm S}$, and $f_{\rm I}$, respectively. Relative error of the temperature for $f_{\rm T}$ and $f_{\rm S}$ was about 5–10%

The first type will be called "a smooth component", the second type, "an impulsive component". For half of the events, more than one (2 or 3) smooth component was detected (see Table 2 and Fig. 2).

The smooth and the impulsive components have been separated by subtracting a constant background, $f_{\rm B}$:

$$f_{\rm T}(t) = f(t) - f_{\rm B} \quad (1)$$

and filtering out the impulsive component. For this purpose, central-moving-averages were used with time-series of the half of the $FWHM$ duration. The result of the averaging was then scaled to the minima of the total HXR flux, $f_{\rm T}$. This gave an estimate of the HXR flux of the smooth component, $f_{\rm S}$, which was subsequently subtracted from the total HXR flux to define the flux $f_{\rm I}$ of the impulsive component.

$$f_{\rm I}(t) = f_{\rm T}(t) - f_{\rm S}(t). \quad (2)$$

Examples of the separation of the smooth and the impulsive component are presented in Figs. 1 and 2.

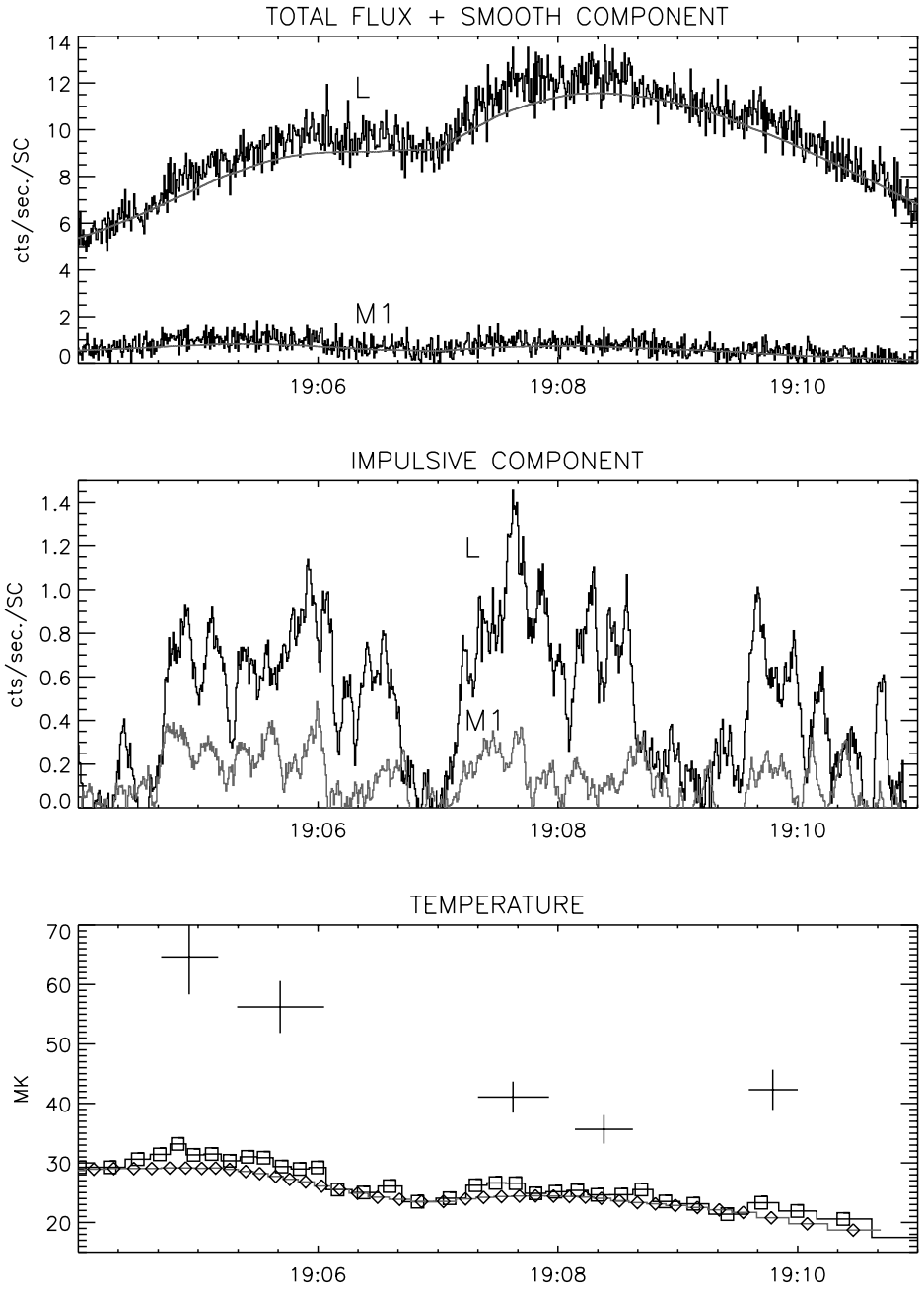

Fig. 2. The HXT light curves of the 13 January 1992 flare (event No. 3) in the channels L and $M1$ (two upper panels) and the temperatures estimated from the $M1/L$ hardness ratio (bottom panel) are presented. The background was subtracted. The 7-minutes interval around the maximum was selected when impulses were the strongest. Two different smooth components are seen. For other details – see the caption of Fig. 1

On the basis of this separation several observational characteristics, i.e., peak flux, time of maximum, $FWHM$ duration, time profile, and relative contribution to the total flux have been obtained for both components and for all investigated flares. Results for the individual event are presented in Table 2. Because of greater number of counts, the values obtained in the channel L have better quality.

Smooth components have quasi-symmetrical time profiles. This property allows us to resolve multi-parts smooth components and to estimate their duration if observations were not complete. Obtained values of the $FWHM$ duration were from about 2 min to about 8 min (Table 2).

To lower the statistical noise, the light curves of the impulsive components were smoothed first by central-moving-averages of 5 s duration. The impulsive components consisted of many individual impulses which appeared randomly during the whole evolution of smooth components. Sometimes they grouped into clusters from which it was difficult to isolate individual episodes (e.g. the middle panel in Fig. 2). The number of impulses increases

Table 2. Basic features of HXR light curves of investigated flares

No.	Date	Maximum count rate f [cts/s/SC][a]				Number of smooth components and their $FWHM$ duration[b] [min]		$FWHM$ duration[b] [sec] of impulses	Contribution of impulses[b,c]
		L	$M1$	$M2$	H				
1[d]	21-Oct.-91	51.7	12.5	3.4	9.7	2:	1.5–2, 2.5–3	9.5–16	medium
2	10-Dec.-91	12.8	4.3	2.5	9.2	1:	2.3	5.5–8.5	medium
3	13-Jan.-92	14.8	4.0	2.6	9.5	2:	∼6, ∼7	6–13	weak
4	6-Feb.-92	122.9	18.3	3.6	10.6	2:	∼5, ∼7	13.5–16, 20.5–28	medium
5	19-Feb.-92	19.7	6.8	2.8	9.1	1:	7.5	12–28.5	strong
6[d]	18-Jul.-92	57.8	7.0	2.9	9.6	1:	3–4	5–10.5	weak
7	24-Nov.-92	13.9	6.3	3.1	9.4	1:	2.3	8.5–13.5	medium
8	24-Nov.-92	4.6	3.2	2.6	9.6	1:	8	8.5–9.5	strong
9	24-Nov.-92	4.3	3.1	2.6	9.3	2:	5.5–6, 6	13–19.5	strong
10[d]	24-Nov.-92	23.7	6.3	3.1	9.9	1:	6–7	12.5–23.5	weak
11	1-Feb.-93	39.8	11.9	5.0	10.6	3:	∼1.5, 2–3, ∼5	7.5–8.5, 13.5–24.5	medium
12	11-Nov.-93	9.2	6.7	4.1	11.2	2:	2.3, 6.6–7	5.5–8.5, 12–15.5	strong
13	29-Jan.-94	125.6	35.6	6.3	11.1	2:	4.5–5.5, 2.2	7–17	medium
14[d]	29-Jan.-94	9.4	4.7	3.4	11.3	1:	7.5–9	10.5–17.5	strong

[a] Background included (typically 1–2, 2–3, 2–3, 8–11 for the channels L, $M1$, $M2$, H, respectively).
[b] From light curves in the channel L.
[c] Description: weak ($f_I/f_T < 0.1$), medium ($0.1 < f_I/f_T < 0.2$), strong ($f_I/f_T > 0.2$).
[d] Flare reached its peak during data gap before available HXT observations.

if we consider weaker ones. The impulses were evidently weaker than the smooth component, as their maximum contribution to the total flux only rarely reached about 25–30%. For individual flares the relative contribution of impulses to the total flux was usually similar (Table 2).

Almost all isolated impulses were symmetrical. This property helped resolve impulses for which a rising or decaying wing was superimposed by other impulses. The histogram of the $FWHM$ duration of 104 impulses that have been resolved in all investigated events is shown in Fig. 3. Obtained values fall within the interval of 5–30 s. Shorter durations were more frequent than the longer durations. Impulses shorter than 5 seconds have been smoothed by central-moving-averages of the light curves, so that the short-period cutoff is artificial. As a rule, impulses resolved in the same flare fall within narrower intervals of $FWHM$ duration values than the whole population (Table 2). Therefore, the peaks at 8- and 12-s in the histogram (Fig. 3) can be explained as a result of an observational selection.

In the next step the time evolution of the hardness ratio $M1/L$ for all investigated events was investigated. The calculations have been made for the total flux as well as for the smooth and the impulsive components. In the case of the total flux and the smooth component time accumulation was adopted to lower the relative error of individual values below 5 percent. To achieve this, for one $M1/L$ value 11–18 counts per subcollimator in the channel $M1$ were needed. For the majority of impulses the number of

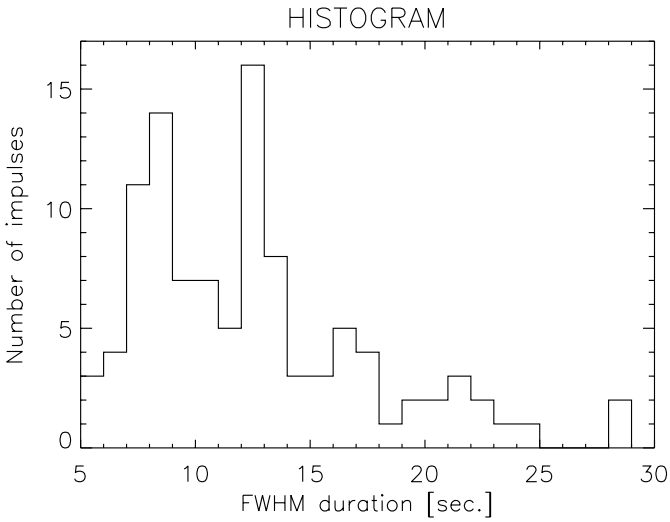

Fig. 3. The histogram of the $FWHM$ duration for 104 impulses that have been found in light curves in the channel L for all investigated events. Central-moving-averages of light curves of 5 s duration have been used. For this reason the cutoff below 7 s is artificial

counts was too low to fulfill such a criterion. Therefore the flux was accumulated over the $FWHM$ duration and one value for one impulse was calculated. For weak impulses the flux was accumulated throughout the whole cluster of impulses. Assuming a specific model of hard X–ray emission and considering the spectral response of the HXT

Table 3. Maximum temperatures [MK] estimated from the $M1/L$ hardness ratio

No.	Total flux[a]	Smooth component[a]	Impulsive component[b]
1	38	34	67
2	37.5	34	60
3	33	29	65
4	38	33	49
5	39	32.5	68
6	26	25	40
7	67.5	59	97
8	28	28	N/A[c]
9	31	31	N/A[c]
10	37	32	94
11	48.5	43.5	92
12	60.5	55	115
13	47	41	87
14	36	32	50

[a] Relative error about 5–10%.
[b] Relative error about 10–20%.
[c] Signal in the channel $M1$ was to weak for reasonable diagnostic.

(Kosugi et al. 1991), the physical condition of emitting plasma was estimated from the calculated hardness ratio. For further presentation of results the hardness ratio $M1/L$ and the fluxes are expressed in terms of the temperature T and the emission measure EM.

Examples of the temperature evolution are presented in bottom panels of Figs. 1 and 2. We see that impulses were responsible for temporal jumps of temperature estimated from the total flux (plots with boxes). After the separation of them, the temperature evolution was smooth (plots with diamonds) and the obtained values were slightly lower. From this observation we can conclude qualitatively that plasma producing impulses was hotter and less frequent than plasma emitting the smooth component. Temperatures obtained from the total flux were mainly within the interval 20–50 MK, only exceptionally reaching higher values, up to 70 MK (Table 3). Temperatures of the smooth component were about several MK lower. The temperatures of the impulses were higher by the factor of 1.2–2.4 than the temperatures estimated for the smooth component (Fig. 4). From the bottom panel of this figure we see that emission measure of impulses were 1–3 orders lower than emission measure of the smooth component.

3. Investigation of images of loop-top hard X–ray emission sources

The HXR light curves have suggested a non-uniform structure of loop-top HXR emission sources. Thanks to the imaging capability of the HXT we can study the origin of the smooth component and the impulses, and find the reasons for the complex character of the smooth component in some events.

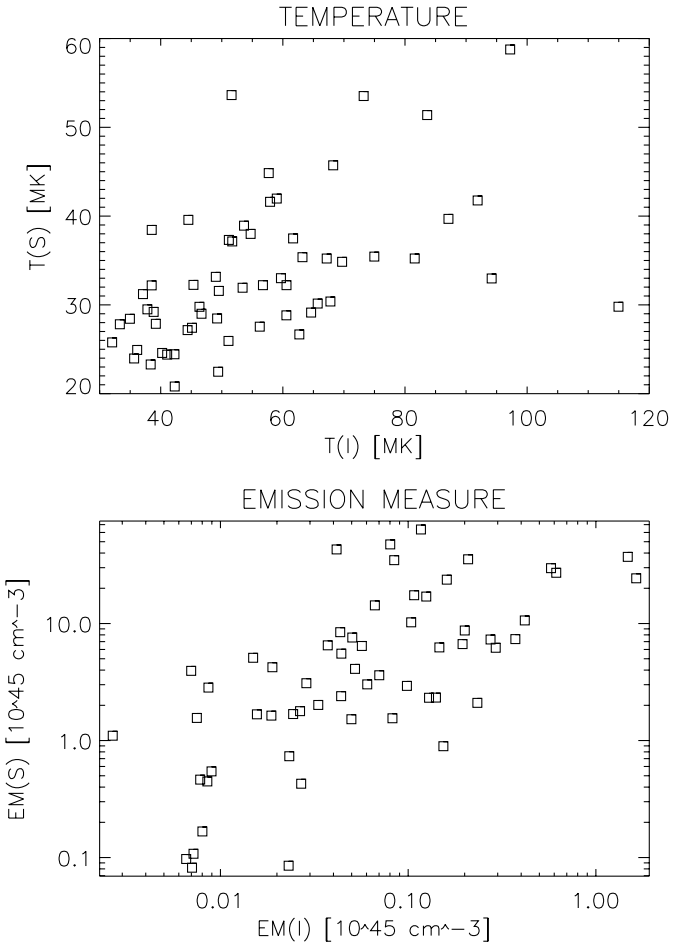

Fig. 4. In the upper panel the plot of the temperature of impulses $T(I)$ versus the temperature of the smooth component $T(S)$ is presented. Values (in 10^6 K units) were calculated from the hardness ratio $M1/L$ for the $FWHM$ duration of impulses or clusters of weak impulses. Relative error was about 10–20% and 5–10% for $T(I)$ and $T(S)$, respectively. In the bottom panel the same plot but for emission measure (in 10^{45} cm^{-3} units) is shown. Relative error was about 20–50% and 15–35% for $EM(I)$ and $EM(S)$, respectively

The *Yohkoh*/HXT images were synthesized using the Maximum Entropy Method adapted by Sakao (1994). The recent HXT instrument response function derived from in-orbit calibrations (Sato 1997) were used. In the channel L all investigated flares had enough counts to synthesize at least five images. In the channel $M1$ this has been achieved for a half of events while in the channel $M2$ only a few images have been obtained for two flares.

The obtained HXR images were compared to the closest in time SXR image derived by the SXT. The accuracy of the coalignment was about 1 arcsec. If we consider the position of HXR emission sources in SXR images, the obtained loop-top sources can be divided into two main types, A and B. Sources of type A are co-spatial with the SXR bright loop-top kernels or "bright knots" (Acton et al. 1992). The SXR counterparts of sources of type B are extended and weak structures situated distinctly higher than bright loop-top kernels. Examples of

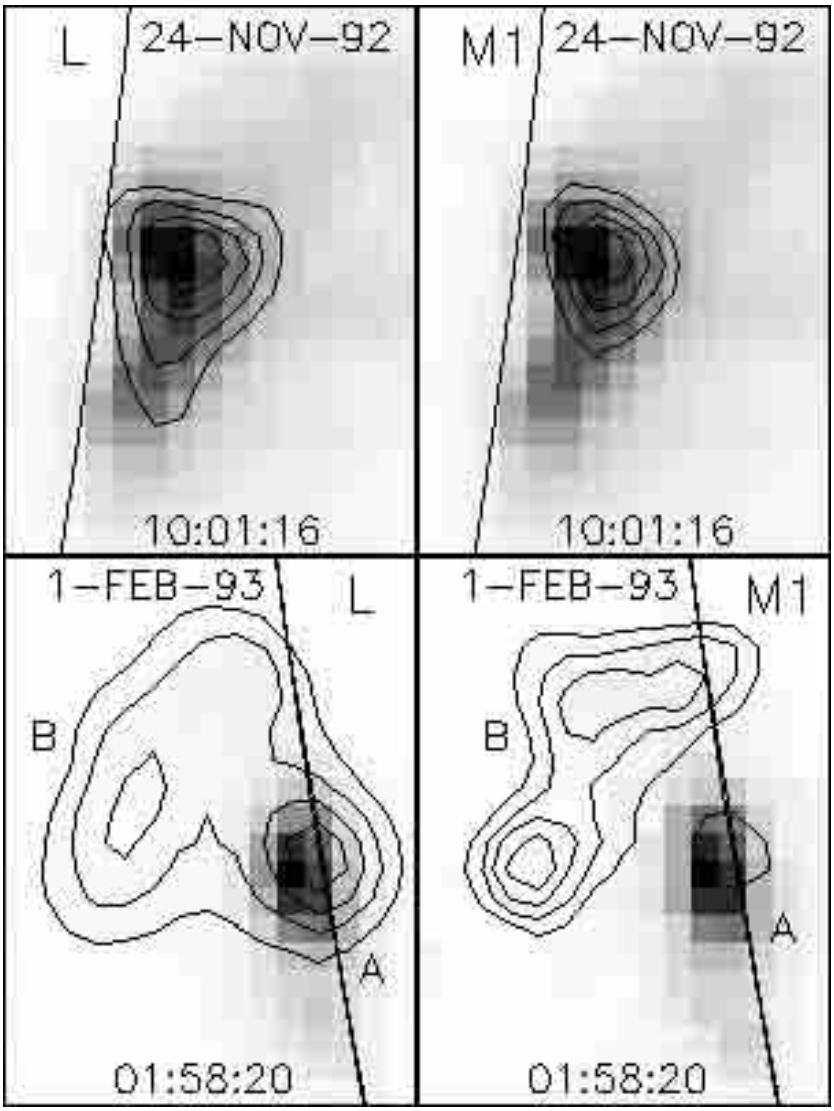

Fig. 5. Examples of the loop-top HXR emission sources. In the upper images of the event No. 7 the source of type A is seen. In the bottom images of the event No. 11 both types of sources, A and B, are shown. In all images solar north is up, east to the left and the size of each pixel is 2.45 arcsec. The SXT(Be119) emission distribution is represented by a grey scale. Contours of the HXR emission (75, 50, 30 and 15% of the maximum intensity) are overplotted in the left images for the channel L and in the right images for the channel $M1$. The times of the SXT(Be119) images are showed. The solar limb is marked by the straight line as a rough guide only

both types of loop-top HXR emission sources are presented in Fig. 5.

The majority of analyzed HXR emission sources were of type A – every flare showed at least one such a source. Sources of type B never existed separately, they always had a companion of type A. The events in which the source of type B occurred always had a complicated magnetic structure and their SXR evolution was prolonged (Table 1). The occurrence of the individual types of sources in the investigated flares is shown in Table 4.

The $FWHM$ shape of the reconstructed HXR emission sources in the channel L was usually constant during the evolution in spite of continuous increase of its height. As a rule, the sources of type A were circular or slightly elongated with the maximum in the middle. A typical diameter was about 5–7 10^3 km (Table 4). A shift between the brightest part of the source of type A and the maximum of the SXR bright loop-top kernel only sporadically was above 2.5 10^3 km. The sources of type B had strongly elongated arch-shape with at least one end reaching the solar limb. The location of the brightest part of the sources of type B changed dynamically from image to image. For this reason and because of the very weak emission of the SXR counterparts, no reliable values of the HXR/SXR shift for the sources of type B have been obtained.

In the channel $M1$ images only minor differences were seen in comparison with the images in the channel L. For example, the $FWHM$ sizes of type A sources were sometimes 10–20 percent lower and the SXR/HXR shift were

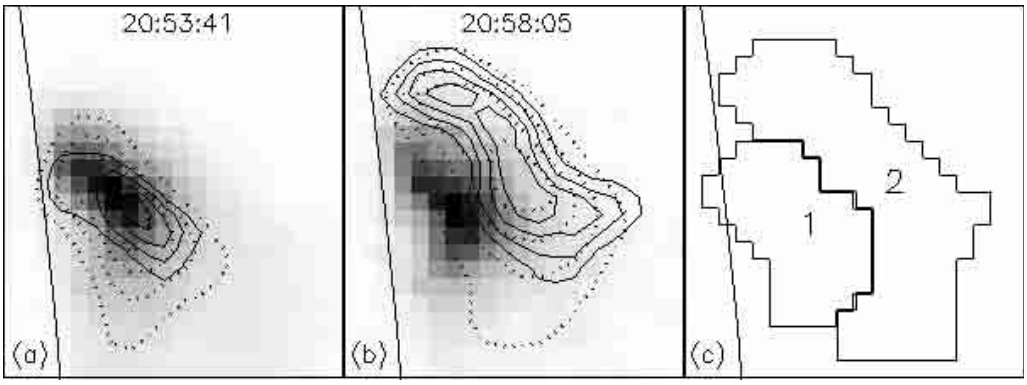

Fig. 6. a,b) Two images of the 6 February 1992 flare (event No. 4) in which two different HXR loop-top emission sources are seen, the first – of type A, and the second – of type B. Contours of the HXR intensity are marked with the solid and dotted lines for the channels $M1$ and L, respectively. For other details – see the caption of Fig. 5. **c)** Regions of interest for which the individual light curves are presented in Fig. 7

Table 4. Morphological characteristics of loop-top HXR emission sources in the channel L

No.	Type of the source	$FWHM$ size[a]	HXR-SXR shift[a]
1	A	2.5 × 3.5	1–1.5
	A	3 × 3.5	< 1
2	A	3 × 4	< 1
3	B	3 × 12	N/A
	A	3 × 3.5	< 1
4	A	4 × 6.5	1–1.5
	B	4.5 × 9	N/A
5	A	3.5 × 8.5[b]	2–2.5
6	A	1 × 3[b]	1–1.5
7	A	3 × 3.5	< 1
8	A	3 × 4	1.5–2
9	A	3 × 3	< 1
	A	2 × 3	1.5–2
10	A	2.5 × 3.5	1–1.5
11	B	3 × 10	N/A
	A	3.5 × 4	< 1
	A	2.5 × 5	< 1
12	A	2 × 3	< 1
	A	3 × 3.5	< 1
13	A	5.5 × 5.5	2–2.5
	B	4 × 7.5	N/A
14	A	3 × 4	1.5–2

[a] In SXT pixels (1 pixel = 2.45 arcsec $\simeq$ 1.8 10^3 km).
[b] Actual shape was cut by the solar limb.

sometimes slightly greater than for the channel L images. In the case of type B sources, a temporal fragmentation occurred (Figs. 5 and 6b) inside the source area seen in the channel L.

The main details of the HXR light curves can be easily identified in the HXR images, i.e., each smooth component has a distinct spatial counterpart in the form of individual HXR emission source. As long as the same source is observed in the HXR images, the HXR light curve shows a single smooth component. If an additional HXR source becomes visible, a separate smooth component in the light curve can be detected. For example, Fig. 6 shows two X–ray images for the 6 February 1992 flare (event No. 4) in which two different HXR emission sources are seen. Individual light curves obtained from the HXR images for the detected emission sources are shown in Fig. 7. We see that each source provides some contribution to the total light curve which can be resolved as consisting of two individual smooth components. The two sources had similar temperatures, about 35 MK, at their peaks of intensity.

Also in other flares, several emission sources in the HXR images were seen when the HXR light curves had several smooth components. However, it was sometimes difficult to separate the sources when they were situated partially along the line-of-sight (events Nos. 1, 3 and 13). For flares with a low number of counts, fewer HXR images were available. Consequently, the light curves for the individual emission sources had less detail than in Fig. 7 and their $M1/L$ diagnostics was more problematic.

Although we can deduce the number of emission sources from the multiple smooth components in the HXR light curve, we cannot obtain more detailed information without imaging. In particular, it is impossible to distinguish between the emission sources of type A and type B on the basis of HXR light curves alone. Considering parameters like the succession of occurrence, maximum flux, $FWHM$ duration, or occurrence of impulses (e.g. see Figs. 2 and 7) we find that very similar smooth components were produced by sources of both types.

It was even more difficult to identify in the HXR images the impulses detected in the HXR light curves. Their duration was usually too short to accumulate enough counts for image synthesis. Therefore, only the strongest impulses offered a possibility to resolve the location in the HXR images where they came from. The images that were obtained during such impulses did not show any additional emission sources in comparison with images that were obtained before and after the impulse. Thus, we conclude that the impulses and the smooth component were emitted from the same sources. In flares with multiple smooth components, the impulses were emitted mainly from the

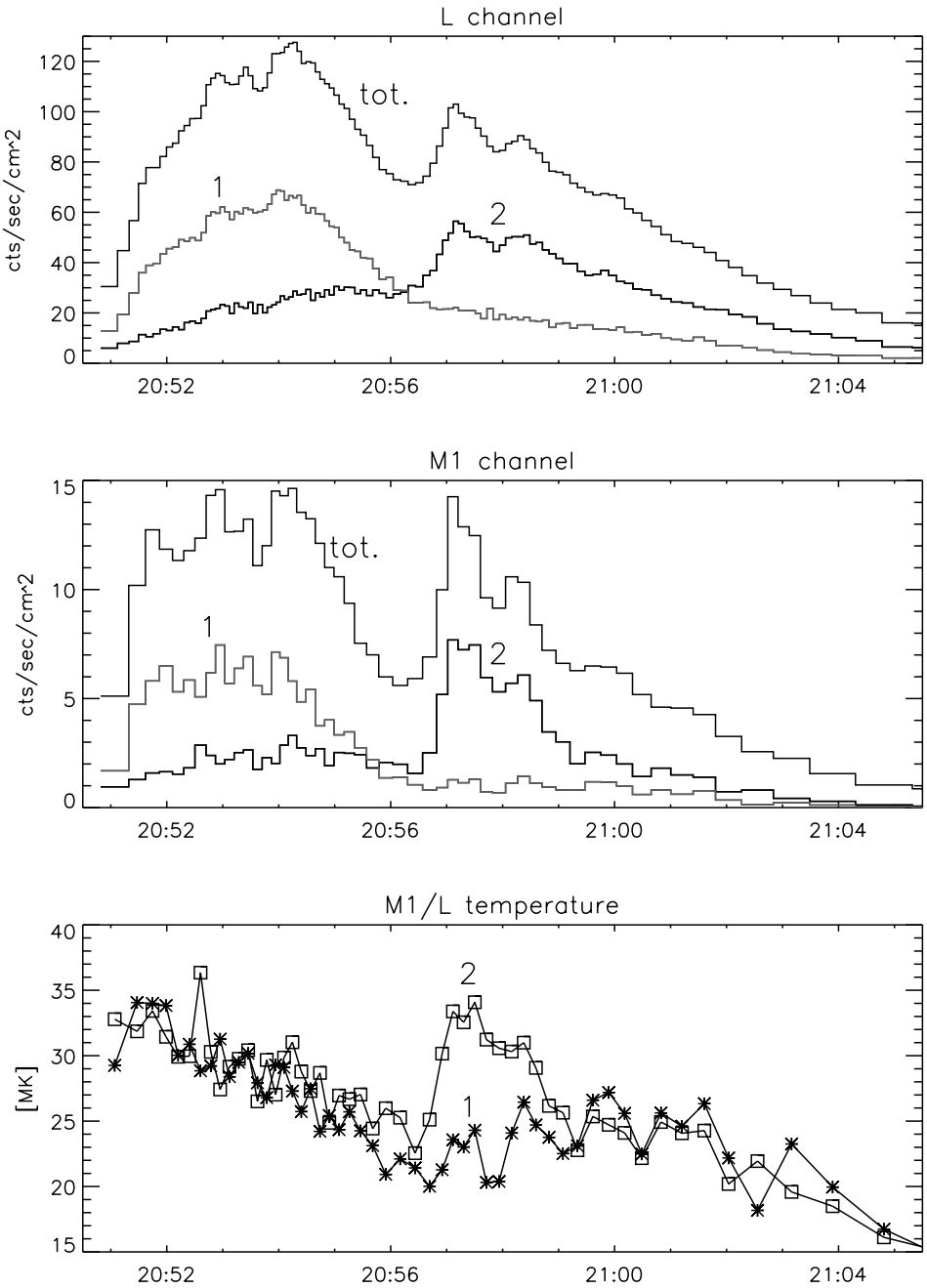

Fig. 7. The HXR light curves of the 6 February 1992 flare (event No. 4) for the total flux and for the individual region of interest which are marked in Fig. 6c. The plots for the channel L (the upper panel) and for the channel $M1$ (the middle panel) are presented. In the bottom panel temperatures estimated from the $M1/L$ hardness ratio are showed. Relative error of the temperature was about 10–15%

source which was the strongest during the time of the impulse (Fig. 7).

4. Comparison with the results of Masuda

Masuda (1994) proposed two different classes of loop-top HXR emission sources: impulsive and gradual. The impulsive sources occur during the impulsive phase simultaneously with the footpoint sources that are evidently stronger. The similar temporal and spectral characteristics suggest the intimate relation of loop-top impulsive sources with the footpoint sources. The gradual loop-top sources are detected in principle after the impulsive phase. They show gradual variation and are much softer than the impulsive sources.

Such a division, however, can be questionable to some extent. First, almost the same area around the SXR loop-top is called either the impulsive HXR emission source or the gradual one, depending on the flare evolution. Moreover, times of accumulation around 10-s or more, that were needed to obtain one HXR image, limited the ability to study short-time fluctuations of loop-top

emission sources. Owing to a lack of definitive evidences for impulsiveness of the impulsive sources some authors (e.g. Kosugi 1994) have called them the loop-top HXR emission sources in the impulsive phase. Finally, as was mentioned in Sect. 1, the presence of stronger footpoint sources could distinctly deform spectral characteristics of impulsive loop-top HXR emission sources.

In this Paper, I selected flares in which footpoint HXR emission sources were occulted by the solar limb. In the absence of footpoint sources it was very difficult to classify the resolved loop-top HXR emission sources as impulsive or gradual, the more so as all obtained sources have showed impulsive and gradual (smooth component) behavior simultaneously. Impulses were the strongest during the maximum of the HXR light curve but they were detectable also far from the maximum. The relative contribution of impulses to the total HXR flux was different for different loop-top sources (Table 2).

All ten flares investigated by Masuda (1994) had gradual HXR emission sources, and seven of them had impulsive loop-top HXR sources. In the present paper, each of fourteen investigated events shows the loop-top HXR emission sources. All sources found by Masuda were single, whereas half of the events in this paper show more than one (2 or 3) different sources. The lower number of loop-top HXR emission sources in Masuda (1994) was probably caused by the dynamical range limit (the footpoint sources were too strong to allow detection of the weaker sources) or/and by the spatial resolution limit of the HXT telescope (the flaring structures were too small to separate individual sources).

If we consider size, shape and connection with the bright loop-top SXR kernels, the loop-top HXR emission sources obtained by Masuda are similar to the type A sources in this paper. The sources of type B do not have any evident equivalent among the sources of Masuda. On the other hand, some of their characteristics suggest a similarity between type B sources and a class of HXR sources called "remote-site impulsive sources" (Kosugi 1994).

Masuda found a relationship between SXR/HXR shift and energy spectrum of the impulsive loop-top HXR emission sources. Three sources showing larger shift (5–10 arcsec), among them the Masuda flare, were more energetic than sources which were almost co-spatial with the bright loop-top SXR kernels. This relationship has not been confirmed for the loop-top HXR emission sources investigated in this paper, e.g., for the two most energetic events, Nos. 7 and 12, their SXR/HXR shift was similar to the coalignment accuracy (Table 4).

If we compare energy spectra of loop-top HXR emission sources presented by Masuda and in the present paper, a fairly good similarity is seen with the exception of three impulsive sources showing the large SXR/HXR shifts, mentioned in the previous paragraph. The maximal temperatures estimated for them from the hardness ratio $M1/L$ were within the interval 108 – >250 MK, that is far above the values obtained in this paper including the most energetic impulses (Table 3).

Two possible explanation of the reported difference should be mentioned. First, the impulsive loop-top sources showing such high-energy spectra were formed in a special magnetic configuration that occurs only exceptionally in the corona. Second, the strong footpoint HXR sources that were observed simultaneously have deformed the real temperature values of the impulsive loop-top HXR source which actually were similar to those obtained in the present paper. Further progress in the HXR image reconstruction as well as more comprehensive survey of behind-the-limb flares with occulted footpoints is needed to decide which explanation is correct.

5. Model of loop-top hard X–ray emission source

Aschwanden et al. (1996b) notice that HXR light curves of many solar flares show two kinds of variability: the smoothly varying and the pulsed fine structure. They argued that the first component was generated either by coronal energy loss during trapping or by chromospheric emission after escaping (trap+precipitation). The pulsed component was produced by electrons precipitated directly without bouncing (direct precipitation).

The smooth and impulsive components were present in HXR light curves of flares investigated in the present paper, however the physical interpretation proposed by Aschwanden et al. (1996b) cannot be adopted. Because of their behind-the-limb location, any radiation of electrons that precipitated into the chromosphere was not seen by the HXT telescope. Therefore, we have to find another explanation of impulses in HXR light curves that are localized in the coronal part of flares.

All loop-top HXR emission sources occupied only a part of the coronal magnetic structures seen in soft X–rays. Following Tsuneta et al. (1997), I have calculated some characteristics of electrons generating the observed hard X–ray radiation. First, the column density, $N_{\rm s}$, needed to stop the non-thermal electrons that radiated within the channels L and $M1$ was estimated using the formula

$$N_{\rm s} = 8.3\ 10^{17}\, E^2 \qquad (3)$$

where E[keV] is energy of electrons. On the other hand, the actual column density, $N = n_{\rm e}\, l$, was calculated. As l the longer size of the loop-top HXR emission source was taken from Table 4. The electron density, $n_{\rm e}$, averaged over the whole area of the loop-top HXR source was estimated from the SXT emission measure map. The obtained values of the ratio $N_{\rm s}/N$ are of about 5–100. This means that electrons should undergo this number of bounces within the loop-top area to be effective in HXR emission.

The above consideration shows that for the electrons emitting the observed hard X–rays a confinement mechanism is needed to keep the particles within the loop-top area where enhanced HXR emission was observed. A presence of a magnetic trap at the location of the loop-top HXR source seems to be the most probable explanation.

However, a typically assumed explanation employing magnetic mirrors as a consequence of the magnetic field convergence can be used only for the loop-top HXR emission sources of type B. Tsuneta et al. (1997) proposed another scheme of the magnetic trap in which the mirrors are the two slow shocks attached to the reconnection X-point. This scheme can be adopted for some sources of type A in this paper. However, such a scheme needs the special overall magnetic structure which cannot be found in the all investigated events.

The turbulent flare kernel model (Jakimiec 1998; Jakimiec et al. 1998) offers another possibility to confine high-energy electrons in a small volume of the corona. In this model, an MHD turbulence develops by multiple magnetic field reconnections in a volume between three magnetic flux tubes (triple magnetic configuration) in the corona above an active region. The topological property of such a configuration leads to the cascade chaotization of the magnetic field inside the volume of the interaction – each magnetic field line being the result of a reconnection will meet a next field line with which it can reconnect. Finally, many transient current sheets will develop in which the magnetic energy will be dissipated very efficiently.

The magnetic field lines inside the turbulent kernel are tangled while the external magnetic field is laminar. Many reconnections decrease the internal field, since the external magnetic field should be somewhat stronger. Due to this and to the fact that inside the turbulent kernel the non-thermal electrons are transported mainly by turbulent motions, we obtain the very efficient mechanism of the confinement. The turbulence will continuously interact with the surrounding magnetic field. Each reconnection in the boundary layer temporarily opens the kernel. However, as estimated by Jakimiec (1999), thickness of the opening is of the order of 10^1–10^2 km. Hence the non-thermal electrons can easily escape only from the thin boundary layer of the turbulent kernel.

The energy released in the turbulent flare kernel heats and maintains a large amount of plasma at high temperature and accelerates a part of electrons to higher energies. In the SXR images we recognize such a place as the bright loop-top kernel, in the HXR images – as the loop-top emission source.

It will be shown that the loop-top HXR emission sources of type A can be treated as the turbulent flare kernels and that the application of this model allows to explain their features presented in Sects. 2 and 3. First of all, they were really turbulent, i.e., their SXR spectra obtained by the BCS showed significant non-thermal line broadening (Khan et al. 1995; Mariska et al. 1996; Mariska & McTiernan 1999). This has been verified for each investigated flare, with the exception of event No. 12 for which there is no BCS data. Moreover, the comment of Khan et al. (1995) that the end of the hard X–rays coincided with the time when the non-thermal line broadening stopped decreasing has found the confirmation for events from the present survey.

Since magnetic energy dissipation in the turbulent kernel occurs in many transient current sheets, it allows to expect that the energy release occurs in portions rather than in continuous way. Kliem et al. (1998) have shown that electrons can be very efficiently accelerated by the induced electric field near reconnection X-points. Since the thickness of the acceleration region is very small ($\sim 10^1$–10^2 m), the number of electrons accelerated in a single current sheet is too low to generate the HXR flux that would be resolved as a separate impulse by the HXT telescope. Taking this into consideration we can explain the smooth and impulsive component in HXR light curves of the loop-top emission sources as follows. The smooth component is produced by overlapping spikes radiated by electrons that were accelerated in individual current sheets that occurred almost uniformly in time. Each impulse that has been resolved by the HXT is generated by a temporal accumulation ("cluster") of current sheets. The presence of impulses shows that the occurrence of the current sheets in the turbulent kernel changes dynamically in time.

Some features of the loop-top HXR emission sources investigated in this paper allow to modify the turbulent flare kernel model. Considering the behind-the-limb location with occulted footpoints of the analyzed events, one can expect that HXR emission of electrons which have escaped from the turbulent kernel is lost, unless the magnetic mirror exists in the upper chromosphere. As was suggested before, it could be the case for the type B sources where an additional acceleration mechanism of electrons should be employed.

Analyzing the SXT temperature maps, Jakimiec et al. (1998) found that the temperature distribution is flat, i.e. $T \simeq$ const at the central parts of the flare kernels. They concluded that the energy release is enhanced near the kernel edges where the turbulence interacts with the stronger, external magnetic field. The presence of impulses in HXR light curves for almost the whole duration of the loop-top emission sources proves that some portion of energy is released still inside the kernel, far from the boundary layer.

6. Conclusions

In this paper the HXT observations of 14 behind-the-limb flares with occulted footpoints has been analyzed. The basic conclusions can be summarized as follow.

Obscuring of strong footpoint HXR emission sources allows to investigate the loop-top sources in more detail. Reconstructed images provide more reliable photometry of such sources.

All investigated flares showed relatively soft, quasi-thermal HXR radiation which was concentrated in the low energy channels (below 33 keV). The HXR light curves had generally smooth shape (the smooth component) with some randomly occurring impulsive spikes (the impulsive component) which were more energetic. Both components were emitted from the same emission source. For half of

the events the smooth component consisted of two or three parts and similar number of emission sources was observed.

Two different types of the loop-top HXR emission sources have been found. Type A sources, detected in each event, are co-spatial with the SXR bright loop-top kernels and have quasi-circular shape. Type B sources have strongly elongated shape, are co-spatial with very weak SXR structures, and occur in complex active regions. No other characteristics, except morphological, differentiate between the sources of types A and B.

The turbulent flare kernel model explains main observational characteristics of the loop-top HXR emission sources of type A: random motions seen as the non-thermal line broadening of SXR lines, confinement of electrons which generate hard X–rays, the smooth and the impulsive component of the HXR light curves. The sources of type B have probably a different origin. Any explanation of type B sources should account for the following features: an additional acceleration mechanism of electrons, the magnetic mirrors in the upper chromosphere, the prolonged evolution of flares showing this kind of sources.

The proposed classification of the loop-top HXR emission sources seems to be more physical than that of Masuda who actually resolved two phases of evolution of the same loop-top source. Moreover, their time variability and energy spectra – the additional criteria of the classification – were probably deformed by strong footpoint sources.

Further studies of the loop-top HXR emission sources are urgently needed, including a more complete survey of the behind-the-limb flares with occulted footpoints, improvement of HXR image reconstruction techniques as well as new sources of data e.g. HESSI.

Acknowledgements. The *Yohkoh* satellite is a project of the Institute of Space and Astronautical Science of Japan. I thank Professor J. Jakimiec for many useful comments and discussions. I thank also Dr. A. Fludra for comments on the manuscript. This work was supported by the KBN grant No. 2 P03D 016 14.

References

Acton, L. W., Feldman, U., Bruner, M. E., et al. 1992, PASJ, 44, L71
Alexander, D., & Metcalf, T. R. 1997, ApJ, 489, 442
Aschwanden, M. J., Hudson, H. S., Kosugi T., & Schwartz, R. A. 1996a, ApJ, 464, 985
Aschwanden, M. J., Wills, M. J., Hudson, H. S., Kosugi, T., & Schwartz, R. A. 1996b, ApJ, 468, 398
Hori, K., Yokoyama, T., Kosugi, T., & Shibata, K. 1997, ApJ, 489, 426
Jakimiec, J. 1998, Publ. Czech Astron. Inst., 88, 124
Jakimiec, J., Tomczak, M., Falewicz, R., Phillips, K. J. H., & Fludra, A. 1998, A&A, 334, 1112
Jakimiec, J. 1999, ESA SP-448, 729
Khan, J. I., Harra-Murnion, L. K., Hudson, H. S., Lemen, J. R., & Sterling, A. C. 1995, ApJ, 452, L153
Kliem, B., Schumacher, J., & Sklyar, D. R. 1998, Adv. Space Res., 21(4), 564
Kosugi, T., Makishima, K., Murakami, T., et al. 1991, Sol. Phys., 136, 17
Kosugi, T. 1994, in Proc. of Kofu Symposium, ed. S. Enome, & T. Hirayama, NRO Report, 360, 11
Mariska, J. T., Sakao, T., & Bentley, R. D. 1996, ApJ, 459, 815
Mariska, J. T., & Doschek, G. A. 1997, ApJ, 485, 904
Mariska, J. T., & McTiernan, J. M. 1999, ApJ, 514, 484
Masuda, S. 1994, Ph.D. Thesis, University of Tokyo
Masuda, S., Kosugi, T., Hara, H., Tsuneta, S., & Ogawara, Y. 1994, Nature, 371, 495
Masuda, S., Kosugi, T., Hara, H., et al. 1995, PASJ, 47, 677
Metcalf, T. R., Hudson, H. S., Kosugi, T., Puetter, R. C., & Piña, R. K. 1996, ApJ, 466, 585
Ohyama, M., & Shibata, K. 1997, PASJ, 49, 249
Piña, R. K., & Puetter, R. C. 1993, PASP, 105, 630
Sakao, T. 1994, Ph.D. Thesis, University of Tokyo
Sato, J. 1997, Ph.D. Thesis, Graduate Univ. Advanced Studies
Shibata, K., Masuda, S., Shimojo, M., et al. 1995, ApJ, 451, L83
Sterling, A. C., Harra-Murnion, L. K., Hudson, H. S., & Lemen, J. R. 1996, ApJ, 464, 498
Tsuneta, S. 1996, ApJ, 456, 840
Tsuneta, S., Masuda, S., Kosugi, T., & Sato, J. 1997, ApJ, 478, 787
Yokoyama, T., & Shibata, K. 1998, ApJ, 494, L113